HHS Public Access

Author manuscript

Neurobiol Dis. Author manuscript; available in PMC 2015 October 01.

Published in final edited form as:

Neurobiol Dis. 2014 October ; 70: 224–236. doi:10.1016/j.nbd.2014.06.023.

Rapamycin improves peripheral nerve myelination while it fails to benefit neuromuscular performance in neuropathic mice

Jessica Nicks[1], **Sooyeon Lee**[1], **Andrew Harris**[1], **Darin J. Falk**[4], **Adrian G Todd**[4], **Karla Arredondo**, **William A. Dunn Jr**[3], and **Lucia Notterpek**[1,2,3]

[1]Department of Neuroscience, College of Medicine, McKnight Brain Institute, University of Florida, Gainesville, FL 32610

[2]Department of Neurology, College of Medicine, McKnight Brain Institute, University of Florida, Gainesville, FL 32610

[3]Department of Anatomy and Cell Biology, College of Medicine, McKnight Brain Institute, University of Florida, Gainesville, FL 32610

[4]Department of Pediatrics, College of Medicine, McKnight Brain Institute, University of Florida, Gainesville, FL 32610

Abstract

Charcot-Marie-Tooth disease type 1A (CMT1A) is a hereditary peripheral neuropathy characterized by progressive demyelination and distal muscle weakness. Abnormal expression of *peripheral myelin protein 22* (PMP22) has been linked to CMT1A and is modeled by Trembler J (TrJ) mice, which carry the same leucine to proline substitution in PMP22 as affected pedigrees. Pharmacologic modulation of autophagy by rapamycin in neuron-Schwann cell explant cultures from neuropathic mice reduced PMP22 aggregate formation and improved myelination. Here we asked whether rapamycin administration by food supplementation, or intraperitoneal injection, could alleviate the neuropathic phenotype of affected mice and improve neuromuscular performance. Cohorts of male and female wild type (Wt) and TrJ mice were assigned to placebo or rapamycin treatment starting at 2 or 4 months of age and tested monthly on the rotarod. While neither long-term feeding (8 or 10 months) on rapamycin-enriched diet, or short term injection (2 months) of rapamycin improved locomotor performance of the neuropathic mice, both regimen benefited peripheral nerve myelination. Together, these results indicate that while treatment with rapamycin benefits the myelination capacity of neuropathic Schwann cells, this intervention does not improve neuromuscular function. The observed outcome might be the result of the differential response of nerve and skeletal muscle tissue to rapamycin.

Corresponding author: Lucia Notterpek, Ph.D., Dept. of Neuroscience, McKnight Brain Institute, 1149 Newell Drive, Box 100244, Gainesville, FL 32610-0244, Phone: 352-294-5373; Fax: 352-392-8347; notterpek@ufl.edu.

Financial Interests or conflicts: None

Keywords

demyelination; autophagy; Schwann cell; myelin; Trembler J; Charcot-Marie-Tooth disease

Introduction

Charcot-Marie-Tooth (CMT) neuropathies comprise a heterogeneous group of disorders that affect approximately 1:2500 (Skre, 1974). The most common form is CMT type 1A, which is typically linked with duplication of the peripheral myelin protein 22 (PMP22) gene, though point mutations in PMP22 have also been identified (Young and Suter, 2003). The Trembler J (TrJ) mouse harbors the same point mutation in PMP22 that is found in a cohort of CMT1A patients (Suter et al., 1992). Nerves of affected mice show demyelination, degenerating axonal profiles, increases in extracellular tissue deposits and Schwann cell hyperproliferation (Notterpek et al., 1997). With age and disease progression, affected mice develop neuromuscular deficits, which are paralleled by degenerative changes at the neuromuscular junction (NMJ) and distal muscle atrophy (Nicks et al., 2013).

PMP22 is a tetraspan constituent of the Schwann cell membrane that has a high propensity to aggregate (Pareek et al., 1997). When the amount of newly-synthesized PMP22 destined for degradation exceeds the capacity of the proteasome, misfolded PMP22 accumulates in cytosolic aggregates (Fortun et al., 2003, Fortun et al., 2007). Similar cellular pathology has been observed in nerve samples from PMP22-linked neuropathic patients (Nishimura et al., 1996, Hanemann et al., 2000), as well as animal models (Fortun et al., 2003, Fortun et al., 2006). Approaches to prevent the accumulation of misfolded proteins within cells include enhancement of the autophagy-lysosomal pathway (Kubota et al., 1999) either with small compounds, or through calorie restriction (Mattson, 2008). Identification of safe and effective calorie restriction mimetic for the treatment and prevention of age-related neural disorders is of great interest (Ingram et al., 2006). Among molecules tested, rapamycin has yielded promising results through the activation of autophagy (Sarkar and Rubinsztein, 2008, Rubinsztein et al., 2012). Rapamycin and its analogs are also of interests as anti-aging therapeutics, which are supported by longevity studies in yeast, worms, flies and mammals (Lamming et al., 2013).

Rapamycin, a lipophilic macrolide antibiotic, inhibits the mammalian target of rapamycin (mTOR) complex (Chong et al., 2012). mTORC1 is involved in nutrient sensing and negatively regulates autophagy (Kim et al., 2013). The activation of autophagy through rapamycin was shown to have positive effects in animal models of Huntington's (Ravikumar et al., 2004), Parkinson's (Malagelada et al., 2010) and Alzheimer's diseases (Caccamo et al., 2010), and also aided myelin expansion by neuropathic Schwann cells in culture (Rangaraju et al., 2010). The positive influence of rapamycin on Schwann cell myelination was dependent on an intact autophagy pathway as ablation of the essential autophagy gene Atg12 diminished the benefits.

In this study, we asked if the beneficial effects of rapamycin on myelination would transfer to animal models of peripheral neuropathies. To test this we administered rapamycin to mice either by dietary supplementation (Harrison et al., 2009, Zhang et al., 2013), or injection

(Meikle et al., 2008). Here we show that while rapamycin improved peripheral nerve myelin content, it did not provide functional benefits to neuropathic mice.

Materials and methods

Mouse colonies

Male and female wild-type (Wt) and heterozygous Trembler J (TrJ) mice on the C57Bl/6J background (The Jackson laboratory) used in the experiments were offspring littermates from our breeding colony maintained in the University of Florida McKnight Brain Institute animal facility under specific pathogen-free (SPF) conditions, on a 7:00 AM–7:00 PM light cycle. The University of Florida Institutional Animal Care and Use Committee approved the use of laboratory animals for these studies. For genotyping, DNA was isolated from tail biopsies of less than 8 day old pups and used for PCR (Notterpek et al., 1997).

Rapamycin administration

Rapamycin diet—Rapamycin-containing food pellets, with the drug encapsulated in a thermoplastic coating using spinning disk atomization, were purchased from Southwest Research Institute and administered at 14 mg per kg of food (2.24 mg rapamycin/kg body weight per day) (Harrison et al., 2009). Placebo diet was constructed the same way, excluding the rapamycin. Age-matched Wt and TrJ littermates were randomly assigned to a placebo or rapamycin-enriched diet at 2 or 4 months of age and fed until reaching 12 months. Mice had ad libitum access to food. Food consumption was monitored per cage to determine the approximate dose per mouse. The body weight of each mouse was measured weekly.

Intraperitoneal rapamycin injection—Rapamycin was obtained from LC laboratories, dissolved at 20 mg/ml in ethanol, and stored at −20°C. Two cohorts of Wt and TrJ mice were injected with rapamycin or vehicle, starting at 2 months of age. Prior to each administration, the stock solution was diluted in 5% Tween 80, 5% polyethylene glycol 400 (both from Sigma), and sterile saline solution (Meikle et al., 2008). The same solution without rapamycin was used as a vehicle control. Rapamycin was administered at 6 mg/kg, 2 times weekly. Mice were injected for 2 months and body mass was measured and recorded before each injection. After two months on the rapamycin regimen, TrJ mice lost over 15% body mass, which prompted us to terminate the study. At 4 months of age, the mice were sacrificed 24 hours after the final injection and blood and tissue samples were collected immediately.

Quantification of rapamycin

Rapamycin was quantified in blood plasma using High Performance Liquid Chromatography/Mass Spectrometry/Mass Spectrometry (HPLC/MS/MS) with ascomycin as an internal standard. Calibration samples were prepared in drug-free human plasma using serial dilutions. The internal standard and precipitation solution was ascomycin at a concentration of 35 ng/ml in 70/30 Methanol/HPLC water with 0.3 M Zinc sulphate. The internal standard solution was added to calibration and experimental plasma samples to precipitate the proteins. An injection volume of 30 μl was used in a Phenomenex Polar RP

50 mm × 4.6 mm × 4 μm. This was followed by mass spectrometry using a Thermo TSQ Quantum Ultra. The ion source was a heated electrospray. Rapamycin ion used was [M $+NH_4^+]^+$, m/z 931.6 and ascomycin ion was $[M+NH_4^+]^+$, m/z 809.5.

Behavioral assessment

Locomotor function was assessed as described (Madorsky et al., 2009). The mice were trained for 2 days on a non-accelerating rotarod (Ugo Basille) set at 5 rpm. On the third day, animals were tested on an accelerating rotarod, starting at 4 rpm and continuing to 30 rpm over a 5 minute period. The mice performed 3 trials with a 1 hour rest between trials and the latency to fall was recorded. Testing was performed at the beginning of each study and then monthly thereafter.

Morphological studies

Proximal ends of the left sciatic nerves from Wt and TrJ mice were prepared for morphological analyses (Madorsky et al., 2009). Samples were fixed in 2% paraformaldehyde and 1% glutaraldehyde in Tyrode's buffer (pH 7.4), treated with 2% OsO4 in 0.1 M sodium cacodylate (pH 7.5), dehydrated and embedded in Spurr's medium. Semi-thick (0.5 μm thickness) sections were stained with toluidine blue and imaged using a SPOT camera attached to a Nikon Eclipse E800 microscope. For the morphometric studies, samples from 4–6 mice per group were evaluated. We used NIH Image J to measure cross-sectional areas of nerve and muscle fibers, and axon diameters. G ratios were calculated as values of axon diameter/fiber diameter (axon plus myelin). To determine the percentage of nerve cross sectional area occupied by fibers, the sum of individual fiber areas were subtracted from the total fixed area (0.04 mm^2 per field). Within the same area, the percentage of myelinated axons relative to total was determined. Statistical analyses were performed using Graphpad prism software.

Immunolabeling studies

Whole soleus muscles were slowly frozen in liquid nitrogen cooled Optimal Cutting Temperature (OCT) gel and sectioned at 20 μm thickness for neuromuscular junction (NMJ) staining, or at 10 μm thickness for incubation with anti-dystrophin antibodies. Sciatic nerve sections (5 μm thickness) from 12-mo old Wt and TrJ mice were processed for immunostaining with polyclonal anti-p62 antibodies, as described (Fortun et al., 2006). Samples were fixed in 4% paraformaldehyde, followed by permeabilization with 100% methanol at −20°C for five minutes. Sections were blocked for 1 hour at room temperature (20% normal goat serum in PBS), then incubated in the indicated primary antibodies overnight at 4°C. Bound primary antibodies were detected with the appropriate fluorescein-conjugated secondary antibodies (1:500), or reacted with Alexa Fluor 594-conjugated α-bungarotoxin (α-Btx) (Invitrogen, 1:500). Hoechst dye (Molecular Probes) was used to identify nuclei, and slides were mounted with an anti-fade kit (Promega). Samples were imaged on a Nikon Eclipse E800 microscope equipped with a Spot camera, or an Olympus DSU spinning disc confocal with deconvolution applied by Slidebook software using the nearest neighbors algorithm. The following criteria were used to categorize neuromuscular junction integrity (Nicks et al., 2013). Fully-innervated junctions show complete apposition of post synaptic sites by the nerve terminal (neurofilament-heavy chain; NFH, 1:2000);

Partially denervated neuromuscular synapses have noticeable thinning of distal nerve fibers (50% of age-matched normal fibers) and retracted or bulging presynaptic terminals; Vacant synapses contain visible acetylcholine receptor sites without innervation by nerve fibers. After categorizing each NMJ, the percentage of each type within individual samples was calculated. For muscle fiber diameter measurements, the samples were immunolabeled with anti-dystrophin (Abcam, 1:250) and analyzed using Image J software. At least 40 fibers per muscle from 4 animals per group were evaluated.

Biochemical analyses

Frozen sciatic nerve, liver, and soleus muscle tissues were crushed under liquid nitrogen and solubilized in lysis buffer (62.5 mM Tris, pH 6.8, 10.0% glycerol, 3.0% SDS) supplemented with protease (Pierce) and phosphatase inhibitors (Sigma). Total protein concentrations were measured using BCA assay (Pierce). Equal amounts of protein (20–30 μg/lane) were separated on 7.5%, 10% or 12.5% SDS-polyacrylamide gels under reducing conditions and transferred to Polyvinylidene Fluoride (PVDF) membranes (Bio-Rad Laboratories). Membranes were blocked with 5% non-fat milk in PBS and incubated overnight with primary antibodies. After washing, anti-mouse, anti-rabbit (both from Cell Signaling Technology, Inc.), anti-rat or anti-chicken (from Sigma-Aldrich) HRP-linked secondary antibodies were added for 2 h. Bound antibodies were visualized using an enhanced chemiluminescence detection kit (PerkinElmer Life Sciences). Films were digitally imaged using a GS-710 densitometer (Bio-Rad Laboratories) and were formatted for printing with Adobe Photoshop 5.5. To monitor autophagy, polyclonal antibodies against phospho-S6, total S6, LC3 (Cell Signaling) and monoclonal anti-p62 (Novus) were used. For analyses of myelin proteins, anti-protein zero (P0) (EnCor Biotechnology) and anti-myelin basic protein (MBP) (Millipore) antibodies were employed. Additional antibodies used in the biochemical analyses include P75 neurotrophin receptor (Promega), phospho-histone H3 (pHH3) (Santa Cruz), poly-ubiquitin (pUB) (Dako), glyceraldehyde 3-phosphate dehydrogenase (GAPDH) (Encor), and MuRF1 (Abcam, Santa Cruz).

Detergent fractionation of sciatic nerves

Frozen sciatic nerves were separated into detergent-soluble and -insoluble fractions as described (Fortun et al., 2006). Briefly, one nerve from each animal was crushed under liquid nitrogen, and lysed in immunoprecipitation buffer containing 5 mM EDTA, 1% NP-40, deoxycholate acid, and supplemented with protease and phosphatase inhibitors. The lysates were centrifuged at 4°C for 10 minutes and the supernatant, containing detergent-soluble material, was removed. The remaining pellet was resuspended in 10 mM Tris-HCl with 3% SDS for 10 minutes at room temperature. Both sets of samples were sonicated, and protein content was determined using Bradford assay. Proteins were prepared for western blots, as described above.

Statistical analyses

All statistical analyses were performed using Graphpad Prism software. For behavioral and body weight analyses, a 2-way ANOVA was employed. Results from the biochemical studies and from the nerve and muscle morphometrics were analyzed using unpaired, 2-tailed Student’s t-test.

Results

The effects of a long-term rapamycin-enriched diet on body weight and locomotor performance

In previous independent studies, rapamycin encapsulated into chow was shown to extend the lifespan of male and female mice when administered late in life, without adverse side effects (Harrison et al., 2009, Zhang et al., 2013). As rapamycin is a recognized inducer of autophagy, a target pathway for CMT1A neuropathies (Rangaraju et al., 2010), we adapted this approach for compound delivery to neuropathic mice. Wt and TrJ mice were assigned to 10 month long feeding regimens with either encapsulated rapamycin or placebo (encapsulation material only) starting at 2 months of age. Mice were weighed weekly and checked daily for overall health. In Wt mice, oral administration of rapamycin had no effect on weight gain, while in TrJ mice a greater than 15% reduction in body weight was noted at the end of the study (Figure 1A). No other adverse effects of the rapamycin-enriched diet on the overall health or grooming behavior of the mice were observed in either genotype.

To monitor locomotor capacities, we used the accelerating rotarod which is a validated assay for assessing the functional phenotype of neuropathic mice (Madorsky et al., 2009). At the beginning of the trial, TrJ mice already performed significantly worse than age-matched Wt and were able to stay on the rotarod for only about 100 seconds (Figure 1B). Under the same testing conditions, Wt mice remained on the rotarod for almost 200 seconds. Over the course of the 10 month long trial, neither Wt nor TrJ mice displayed significant changes in locomotor capacities with rapamycin feeding, as compared to placebo (2-way ANOVA). In agreement with the literature (Boger et al., 2011), an age-related decline in performance was detected in both genotypes (2-way ANOVA, $^{\ddagger}p=0.001$).

The effects of rapamycin on mTORC1 in liver and sciatic nerve

To ascertain that rapamycin was absorbed into the bloodstream of compound treated rodents as reported (Harrison et al., 2009, Zhang et al., 2013), we collected blood from each mouse at the end of the study and the concentration of rapamycin was determined using HPLC/MS/MS. In the plasma of placebo-fed mice, rapamycin was below the level of detection, while in the special diet fed group rapamycin was identified at 10–12 ng/mL (Figure 2A). This rapamycin concentration is lower than reported in the original publication on the chow-encapsulated formulation (Harrison et al., 2009, Zhang et al., 2013), but it is near the range found in a recent study with aged C57BL/6Nia mice (Zhang et al., 2013). To monitor the bioactivity of rapamycin, we assessed liver tissue for mTORC1 inhibition, as determined by the phosphorylation state of the ribosomal protein subunit S6 (Figure 2B). As shown on the blot, the levels of phospho-S6 (pS6) are notably reduced in the liver of rapamycin-fed mice, as compared to placebo. Analyses of the ratios of pS6 to total S6 from independent samples reveals statistically significant decreases in S6 phosphorylation in both genotypes (Figure 2C).

Next, we analyzed sciatic nerve lysates from placebo and rapamycin-fed mice for the levels of pS6 and S6, as well as for microtubule-associated protein light chain 3 (LC3) (Figure 2D). As shown on the blot, the rapamycin-enriched diet reduced the levels of pS6, however

upon quantification of pS6/S6 ratios in independent nerve samples this decrease is not significant (Figure 2E). As a measure of autophagic activity, within the same nerve lysates we evaluated the expression of LC3 (Figure 2D). Consistent with our previous reports on increased autophago-lysosomal activity in nerves of TrJ mice (Notterpek et al., 1997, Fortun et al., 2003); in samples from placebo-fed neuropathic animals the total levels of LC3 are elevated, as compared to Wt. During autophagy, LC3 I is lipidated to form the membrane bound LC3 II, and the amount of LC3 II is known to correlate with the number of autophagosomes (Mizushima and Yoshimori, 2007, Parzych and Klionsky, 2013). Analyses of the ratios of LC3 II to LC3 I in independent nerve samples did not reveal a statistically significant change in either genotype (Figure 2F), which might be reflective of reduced demand on the pathway after extended rapamycin consumption.

As an additional measure of autophagic activity we examined the expression of p62, an ubiquitin-binding scaffold protein that binds ubiquitinated substrates and shuttles them to autophagosomes (Ichimura and Komatsu, 2010). Sciatic nerves from neuropathic TrJ mice contain elevated levels of poly-ubiquitinated substrates (Fortun et al., 2003, Rangaraju et al., 2010), and show an abundance of anti-p62 reactive protein aggregates, as compared to Wt (Figure 2G). Upon the rapamycin intervention, an attenuation of this phenotype is noted which is confirmed by biochemical studies (Figure 2H). Indeed, statistical analyses of independent blots detect a significant increase in the levels of p62 in affected mice, as compared to Wt, and diminution of this phenotype by the intervention (Figure 2I). As mentioned above, we have previously described elevated levels of detergent-insoluble ubiquitin-tagged proteasome substrates in nerves of neuropathic mice (Fortun et al., 2006), a finding that is consistent in the current placebo-fed cohort (Figure 2J). As shown on the graphs, there is a statistically significant increase in detergent-insoluble ubiquitin-reactive substrates as well as p62 in nerves of 12-mo old TrJ mice, as compared to age-matched Wt (Fig. 2K, L). Notably, the rapamycin diet was effective in reducing the levels of such undegraded proteasome substrates, as well as the abundance of p62 (Figure 2K, L). Together, these results support the notion that through activation of autophagy, chronic, low dose rapamycin-enriched diet facilitates the removal of undegraded proteasome substrates in nerves of neuropathic mice.

Myelin protein expression and nerve morphology in rapamycin-fed neuropathic mice

In culture, rapamycin was effective in enhancing the myelination capacity of neuropathic Schwann cells, which was reflected in both the number and lengths of myelin internodes (Rangaraju et al., 2010). To examine if rapamycin had a similar effect on myelinated nerves in vivo, we analyzed whole sciatic nerve lysates for the levels of myelin proteins, protein 0 (P0) and myelin basic protein (MBP) (Figure 3A). P0 constitutes approximately 50% of the total protein in peripheral nerve myelin, while MBP is a key molecule in myelin compaction (Martini and Schachner, 1997). In agreement with our previous studies (Notterpek et al., 1997), the steady-state levels of P0 and MBP are significantly reduced in nerves of TrJ mice, when compared to age-matched Wt (Figure 4B, C). Nerve lysates from TrJ mice on the rapamycin-enriched diet however show a notable increase in the expression of these myelin proteins. Upon analyses of independent samples, we found statistically significant improvement in the levels of P0 and MBP in the intervention groups, which is significant for

MBP even in Wt (Figure 3B, C). Besides demyelination, nerves of neuropathic rodents contain supernumerary Schwann cells, as the cells re-enter the cell cycle and express the P75 neurotrophin receptor, a marker of non-myelinated Schwann cells (Jessen and Mirsky, 1999). Indeed, the levels of P75 and pHH3, a mitotic marker, are elevated in samples from placebo fed TrJ mice, as compared to Wt (Figure 4D–F). In response to the intervention, the genotype effect on the expression of P75 and pHH3 is diminished, a finding that is statistically significant across multiple independent samples (Figure 4E, F).

To corroborate the findings from the biochemical analyses (Figure 3), proximal segments of each left sciatic nerve were prepared for morphometric studies. Previously, we detected significant alterations in nerve morphology of TrJ mice, including decreased axonal diameter, increased amounts of extracellular deposits, Schwann cell overproliferation and demyelinated and unmyelinated axons (Notterpek et al., 1997). These abnormalities are pronounced when nerve cross sections from 12 month old placebo-fed Wt and TrJ mice are compared (Figure 4A). While the rapamycin diet did not have an obvious effect on Wt nerves, the micrographs from rapamycin-fed TrJ mice suggest improvements. To confirm this observation, we performed morphometric analyses on nerve cross sections from the 4 experimental groups (Figure 4B–E), including quantification of the percentage of myelinated fibers, nerve tissue area occupied by fibers, measurements of nerve fiber diameter, and calculations of G ratios (Notterpek et al., 1997, Madorsky et al., 2009). In agreement with the previous reports, all 4 of these measurements are affected by the TrJ genotype (Fig. 4B–E, (#$p<0.001$). As suggested by the representative micrographs (Figure 4A), the percentage of myelinated axons in a fixed field of view is significantly increased in rapamycin-fed TrJ mice (Figure 4B, *$p<0.05$). Similarly, we found significant improvements in nerve tissue area occupied by fibers, as well as in fiber diameter (Figure 4C, D). A frequently used index of nerve myelination is the G ratio, which represents the ratio of axon to fiber (myelin + axon) diameter. Significantly, long-term rapamycin-enriched diet is associated with a significant decrease in G ratios in nerves of neuropathic mice, which is indicative of improved myelination (Figure 4E). In accord with the detection of increased MBP levels in samples from Wt mice (Figure 3C), we also detected significant improvements in axon diameters and G ratios on the intervention (Figure 4C–E). Together, these results are in agreement with previous in vitro studies that showed a positive influence of rapamycin on myelin formation by both neuropathic and Wt Schwann cells (Rangaraju et al., 2010, Rangaraju and Notterpek, 2011).

Skeletal muscle innervation in rapamycin-enriched diet fed mice

As shown above, a long-term rapamycin-enriched diet improved the morphology and myelin content of peripheral nerves in neuropathic mice (Figures 2–4), yet the animals did not perform better on the rotarod (Figure 1). This discrepancy between nerve biology and neuromuscular function could be the result of impairments at distal nerve segments, at the neuromuscular junction (NMJ) and/or in skeletal muscle strength. Recently, we described age-associated progressive degenerative changes at distal nerve segments and myofiber atrophy in TrJ mice (Nicks et al., 2013), which prompted us to examine these tissue regions in the current therapeutic study. To evaluate the effects of the rapamycin-enriched diet on the integrity of NMJs, soleus muscle tissue was sectioned and reacted with α-Btx to label

postsynaptic sites and with antibodies to phosphorylated neurofilaments to mark presynaptic terminals (Figure 5A). In agreement with previous studies (Nicks et al., 2013), skeletal muscle of 12-mo old TrJ neuropathic mice contain approximately 60 % normal, fully-innervated, and less than 40 % partially-innervated, and/or vacant NMJs (Figure 5A, B). Using the same methodology we found that the rapamycin-enriched diet had no significant effect on the percentage of NMJs in the three categories (Figure 5B).

Since we did not detect significant improvement or deterioration at the NMJs, we asked if the intervention affected skeletal muscle tissue. To determine if rapamycin was active in skeletal muscle, we examined the expression of pS6 and total S6 (Figure 5C). As indicated by the representative Western blot, the steady-state levels of pS6 and S6 are elevated in muscles from placebo-fed TrJ mice, a phenotype that is significant across independent samples. Since rapamycin had notable effects on the levels of muscle pS6 and S6 in both genotypes (Figure 5C), we did not detect diet-induced, statistically significant changes in the pS6/S6 ratios (Figure 2D). Nonetheless, the decreases in pS6 and S6 in the intervention groups suggest that rapamycin reached the skeletal muscle, which prompted us to examine additional markers of muscle biology. As shown previously (Nicks et al., 2013), MuRF1, a muscle atrophy marker (Bodine et al., 2001, Koyama et al., 2008) is elevated in samples from 12 month old neuropathic mice (Figure 5E). Analyses of independent samples reveal that the genotype-linked increase in MuRF1 levels is not attenuated by the rapamycin intervention (Figure 5F). Next, we measured cross-sectional myofiber areas in the soleus muscle after immunostaining with an antibody to dystrophin (Figure 5G). In accord with previous data (Nicks et al., 2013), we identified a genotype-associated decrease in myofiber diameter in 12 month old TrJ mice, an abnormality that is not affected by the intervention (Figure 5H). Taken together, these results indicate that the long-term rapamycin-enriched diet was not effective in attenuating the muscle pathology in TrJ neuropathic mice, which may have contributed to the lack of improvements on the behavioral tasks.

Elevated levels of circulating rapamycin negatively impacts body weight and locomotor performance in neuropathic mice

Since rapamycin has been shown to provide benefits to mice at the 60–70 ng/ml plasma concentrations (Meikle et al., 2008, Harrison et al., 2009), we asked whether increasing the dose would improve the rotarod performance of affected mice. Based on our in vitro pharmacokinetic studies with rapamycin (Rangaraju et al., 2010), and data from the literature (Meikle et al., 2008, Harrison et al., 2009), we injected Wt and TrJ mice twice weekly with 6 mg/kg of rapamycin beginning at 2 months of age. The body mass of the mice was recorded prior to each injection, and the rotarod test was administered at the beginning of the study, and monthly thereafter. In Wt mice, injection of rapamycin had no significant effect on overall weight gain, however drug-treated TrJ mice showed a significant reduction in body weight after 2 months (*p=0.02, Figure 6A), which led us to terminate the study.

Based on the results from the diet regimen trials, which indicated age-related decline in the ability of TrJ mice to stay on the rotarod (Figure 1B), we lowered the rate of acceleration from 4–35 rpm to 4–25 rpm over a 5 minute period. Using these parameters, Wt mice stayed

on the rotarod for about 250 seconds regardless of whether they were injected with rapamycin or vehicle. In comparison, after 2 months on the regimen TrJ mice injected with rapamycin had a significant impairment in their ability to remain on the rotarod, as compared to vehicle (Figure 6B, *p=0.04). The negative effects of rapamycin injections on the locomotor performance and weight gain of TrJ mice are consistent across three independent trials, which prompted us to terminate the trial when the animals were 4 months old.

At the end of the study, we collected blood from each animal and the concentration of rapamycin in the plasma was determined using HPLC/MS/MS, as above. In comparison to the rapamycin food supplementation trials (Figure 2A), the drug concentrations in the plasma is greater than 60 ng/mL in both Wt and TrJ mice (Figure 6C), which is nearly 6-fold higher than in the feeding trial. To assess the bioactivity of rapamycin, we determined the ratio of pS6 to S6, as an indicator of mTORC1 inhibition. As shown on the western blots, pS6 levels are notably reduced in the liver lysates of rapamycin injected mice, an effect that is significant across independent samples (Figure 7A, B). Lysates of sciatic nerves were similarly analyzed for pS6 and S6 ratios, as well as for the expression of LC3 (Figure 7C). As detected in the samples from 12 month old mice (Figure 2D), there is a genotype effect on the basal levels of pS6 and S6 in nerve lysates of neuropathic mice (Figure 7C). Upon quantification, we found a significant reduction in the pS6/S6 ratios, indicating inhibition of mTORC1 (Figure 7D). In examining the steady-state levels of LC3 we found a genotype effect, however the ratio of LC3II/I is not affected by the intervention (Figure 7C, E). Together these results indicate that rapamycin is bioactive in the liver and sciatic nerve of injected mice, as measured by reduced phosphorylation of S6, a downstream target of mTOR.

Peripheral nerve myelination in rapamycin injected mice

Just after 2 months on the rapamycin injection regimen, TrJ neuropathic mice exhibited a significant decline in locomotor performance (Figure 6). To examine potential causes for the functional deficits, we isolated the sciatic nerves from each mouse and analyzed the levels of myelin proteins, as well as nerve morphology (Figure 8). As expected (Notterpek et al., 1997), Western blot analyses of whole nerve lysates for the myelin proteins P0 and MBP reveal a pronounced genotype effect (Figure 8A), which is significant across independent samples (Figure 8B). Relative to vehicle, nerve lysates from TrJ mice injected with rapamycin show a significant increase in MBP, but not in P0 (Figure 8B). These results indicate that despite the deleterious effects of rapamycin on the rotarod performance of the mice (Figure 6B), the nerves contain more myelin proteins.

To substantiate the biochemical findings, cross sections from proximal nerve segments were prepared for basic morphometric analyses, using the same methodologies as above. The micrographs from 4-month old vehicle and rapamycin injected TrJ mice appear similar, with good preservation of myelinated fibers (Figure 8C). Morphometric analyses of independent nerves support the results from the biochemical studies (Figure 8A) and indicate maintenance of myelinated fibers (Figure 8D), and an improvement in myelin thickness, as determined by reduced G ratio values (Figure 8F). The average nerve fiber diameter

decreased in rapamycin treated TrJ mice, with the larger caliber axons being more affected (Figure 8E). Together, these results are consistent with the findings from the long-term rapamycin feeding studies (Figures 2–4) and indicate that activation of autophagy in nerves of neuropathic mice supports myelination.

Inhibition of mTOR is not beneficial to muscle in neuropathic mice

The primary target of rapamycin is mTORC1, which has been shown to play an important role in muscle protein synthesis and remodeling following acute, injury-induced denervation (Bentzinger et al., 2013, Quy et al., 2013). While muscle denervation is not a prominent pathology in young neuropathic mice (Nicks et al., 2013), it has been suggested that muscle innervation might not develop normally in some neuropathic animals (Meekins et al., 2004). First we assessed the level of mTOR inhibition in whole soleus muscle lysates following two months of rapamycin treatment by examining the steady-state levels of pS6 and S6 (Figure 9A). As shown in the Western blot, there is a notable decrease in pS6 in samples from rapamycin injected mice, an observation that is significant across independent samples (Figure 9B, *p=0.02). To determine if inhibition of mTOR had a measurable effect on muscle health, we assessed the levels of MuRF1 and measured myofiber diameter (Figure 9C–E). Compared to samples from 12 month old animals (Figure 5E, F), the genotype affect is not significant at 4 months, when Wt and TrJ mice are compared. Similarly, we did not find a statistically significant change in the steady-state expression of MuRF1 upon rapamycin injection (Figure 9D). In muscle of 12 month old neuropathic mice, the increased levels of MuRF1 correlate with a decrease in myofiber diameter, as compared to age-matched Wt (Nicks et al., 2013). Therefore we also analyzed myofiber cross-sectional areas in the soleus muscle after staining with anti-dystrophin antibodies, which did not reveal statistically significant changes (Figure 9E). Together, the results indicate that increasing the levels of circulating rapamycin by i.p. injections negatively impacts the neuromuscular performance of young TrJ mice, without obvious deleterious changes in the studied skeletal muscle proteins.

Discussion

The described results are representative of findings from six independent trials with rapamycin across a 3 year time span. Both long-term low dose, orally-administered, and short-term, high dose i.p. injected rapamycin lead to improvements in peripheral nerve myelin content in neuropathic mice, which is consistent at 4 and 12 months of age. These in vivo results are in agreement with our previous in vitro study that illustrated the requirement for the autophagic pathway in mediating the beneficial effects of rapamycin on myelin formation by Schwann cells from neuropathic mice (Rangaraju et al., 2010). The reduction in poly-ubiquitinated proteins in nerve lysates from treated animals is also consistent with the in vitro work that identified rapamycin as an effective drug in clearing intracellular protein aggregates from neuropathic Schwann cells (Fortun et al., 2003, Rangaraju et al., 2010). Compared to Schwann cells, the influence of rapamycin on skeletal muscle biology is more complex. In contrast to the literature (Zhang et al., 2013), we did not find an improvement in rotarod performance of rapamycin-treated 12 month old Wt mice, which could be due to the differences in the ages and/or baseline performances of the test cohorts.

In addition, the response of skeletal muscle to long-term rapamycin supplementation was heterogeneous, while neuromuscular function deteriorated in rapamycin-injected TrJ mice. Together, the results highlight tissue-specific responses to systemic rapamycin administration, which is augmented by the genetic defect in hereditary neuropathic mice.

Concerning the potential use of rapamycin for the treatment of neural disorders it is imperative to discuss the variability among the reported plasma concentrations. In our feeding studies, we employed the same encapsulated rapamycin that has been used in a number of aging studies (Harrison et al., 2009, Zhang et al., 2013). The encapsulation prevents degradation of the enteric coating until it reaches the small intestine. This diet formulation was shown to extend lifespan in a genetically heterogeneous group of mice with plasma rapamycin concentrations ranging from 60–70 ng/mL (Harrison et al., 2009). In another recent aging study with mice on the C57/BL6 background, extension of lifespan was observed in rapamycin-fed animals, however plasma levels were reported at around 4 ng/mL (Zhang et al., 2013). In our 8 or 10 month long feeding studies where the mice had ad libitum access to the rapamycin-enriched chow, plasma levels of the drug were detected at 10–12 ng/mL, which is in between the values of the two previous publications. It has been proposed that there is a potential strain effect on rapamycin absorbance although TrJ mice are bred on the same C57/BL6 background as those used in the latest aging study (Zhang et al., 2013). The method of rapamycin quantification, as well as the age of the mice, are additional variables among the cited in vivo studies, with the later known to affect the absorption and clearance of rapamycin (Meikle et al., 2008).

A consistent effect of rapamycin treatment is the extension of lifespan in multiple organisms (Lamming et al., 2013). A number of potential mechanisms that may mediate this effect are discussed in a recent review in The Journal of Clinical Investigation by Lamming and colleagues (2013) and include autophagy, the target pathway for our studies. Alterations in autophagic activity have been associated with several adult-onset neurodegenerative disorders that involve protein aggregation (Sarkar and Rubinsztein, 2008). PMP22-linked hereditary neuropathies fall in this category as Schwann cells of affected nerves contain ubiquitin-positive protein aggregates and markers of elevated basal autophagy (Fortun et al., 2003, Fortun et al., 2006). Activation of autophagy by dietary modulation has been shown to be beneficial in animal models of protein aggregation disorders, including Alzheimer’s and Parkinson’s diseases, as well as CMT1A neuropathies (Madorsky et al., 2009, Srivastava and Haigis, 2011, Lee and Notterpek, 2013). Through inhibition of mTOR, a well-known regulator of autophagy, rapamycin is considered to be a calorie restriction mimetic and is of great interest in studies of neurodegenerative disorders. However, because of the multiple mechanisms mTOR affects, investigators have reported different outcomes when applying rapamycin or silencing mTOR. For example, during development, mTOR is essential for oligodendrocyte differentiation and CNS myelination (Narayanan et al., 2009, Tyler et al., 2009), as well as for proper myelination of peripheral axons (Sherman et al., 2012). Previously, in our *in vitro* model, we applied rapamycin after the Schwann cells slowed proliferation and were induced to myelinate (Rangaraju et al., 2010). In the current study, we similarly initiated the rapamycin intervention at either 2 or 4 months, an age when developmental aspects of peripheral nerve myelination have been completed and misfolded

proteins begun to accumulate within Schwann cells. Still, the beneficial effects of rapamycin in enhancing myelin content of neuropathic nerves was likely mediated by additional mechanisms besides autophagy, and could involve anti-proliferative and anti-inflammatory mechanisms (Lamming et al., 2013). Indeed, hereditary demyelinating neuropathies are known to involve Schwann cell hypertrophy (Niemann et al., 1999), an abnormality that was mitigated by rapamycin treatment (Figure 3).

Given the beneficial effects of rapamycin on peripheral nerve myelin content in neuropathic mice, why did performance on the rotarod not improve? While this outcome came to us as a surprise in the first trials, the results are remarkably consistent across independent cohorts of mice. As shown in the analyses of NMJs and muscle tissue, rapamycin was ineffective in improving distal nerve target innervation (Figures 5 and 9). While there are limited reports on muscle pathology in hereditary neuropathies, at least two previous studies have identified progressive degenerative changes in distal muscles of TrJ mice, including discernible deficits at 2 months of age (Meekins et al., 2004, Nicks et al., 2013). Currently, the subcellular mechanisms that are activated within muscle cells by the nerve myelin defects in TrJ neuropathic mice are not fully understood. Nonetheless, in acute, injury-induced models of muscle denervation the role of mTORC1 activity in muscle health has been elucidated (Quy et al., 2013). Autophagy was shown to be suppressed in denervated muscle to increase protein synthesis for remodeling, while activation of autophagy by rapamycin enhanced muscle atrophy and increased protein degradation (Quy et al., 2013). Therefore, if one draws analogy between acute and chronic neuropathy-mediated denervation, then it is conceivable that systemic inhibition of mTORC1 and activation of autophagy in skeletal muscle of neuropathic mice could exacerbate muscle degeneration. The results in this article (Figure 5 and 9) support this hypothesis, even though not all examined markers of muscle biology were significantly altered. In addition, it is possible that while myelin protein expression and nerve morphology improved, the intervention had no beneficial effect on nerve conduction velocity, which is critical for neuromuscular function.

The findings from our study support the need for better characterizing the effects of rapamycin and its analogues, including everolimus and temsirolimus in whole animals, as well as the identification of more selective activators of autophagy. Rapamycin and its analogues are FDA-approved compounds and are currently in use for organ transplant patients (Forgacs et al., 2005). It is of note that in a cohort of patients receiving kidney or liver transplants, the conversion to rapamycin as an immunosuppressant reduced neurotoxicity and neuropathic-like symptoms (Forgacs et al., 2005). The FDA clinical trial website lists over 1000 phase I and II clinical trials involving rapamycin, along with its analogues. The fact that rapamycin is involved in many clinical trials for a variety of conditions shows overall drug efficacy and tolerance in humans. Yet, based on our findings related to the differential effects of rapamycin on peripheral nerve and skeletal muscle health, we recommend caution when administering inhibitors of mTORC1, as such drugs could impact skeletal muscle health when nerves are injured (Quy et al., 2013). Utilizing compounds that induce autophagy through mTORC-independent mechanisms could be of significant benefit to neuropathic patients, without impacting muscle biology. One recent study has in fact identified a peptide consisting of a specific sequence of the beclin protein

that induces autophagy and reduces protein aggregation in an *in vitro* model of Huntington's disease (Shoji-Kawata et al., 2013). The efficacy of this pro-autophagy drug in vivo is yet to be tested. Furthermore, better understanding of the autophagic pathway, including identification of the transcriptional program responsible for inducing autophagy and lysosomal proteins (Klionsky and others, 2012), will facilitate this effort. Alternatively, approaches to target rapamycin and/or its analogues specifically to Schwann cells would alleviate off-target effects in other tissues.

Acknowledgments

The authors wish to thank Irina Madorsky, Amanda Sookdeo and Kathryne Kostamo for their assistance with the rodent studies, members of the Notterpek lab for thoughtful discussions and Dr. Timothy Garrett and the Biomedical Mass Spectrometry core for the HPLC analysis. The NIH-NINDS, the Facial Pain Research Foundation and Tom and Susie Wasdin provided support for these studies.

Abbreviations

TrJ	Trembler J
PMP22	peripheral myelin protein 22
RM	rapamycin
NMJ	neuromuscular junction
SDS	sodium dodecyl sulfate
P0	protein zero
MBP	myelin basic protein
PBS	phosphate buffered saline
NFH	neurofilament-heavy
MuRF1	muscle ring-finger protein 1

References

Bentzinger CF, Lin S, Romanino K, Castets P, Guridi M, Summermatter S, Handschin C, Tintignac LA, Hall MN, Ruegg MA. Differential response of skeletal muscles to mTORC1 signaling during atrophy and hypertrophy. Skelet Muscle. 2013; 3:6. [PubMed: 23497627]

Bodine SC, Latres E, Baumhueter S, Lai VK, Nunez L, Clarke BA, Poueymirou WT, Panaro FJ, Na E, Dharmarajan K, Pan ZQ, Valenzuela DM, DeChiara TM, Stitt TN, Yancopoulos GD, Glass DJ. Identification of ubiquitin ligases required for skeletal muscle atrophy. Science. 2001; 294:1704–1708. [PubMed: 11679633]

Boger HA, Mannangatti P, Samuvel DJ, Saylor AJ, Bender TS, McGinty JF, Fortress AM, Zaman V, Huang P, Middaugh LD, Randall PK, Jayanthi LD, Rohrer B, Helke KL, Granholm AC, Ramamoorthy S. Effects of brain-derived neurotrophic factor on dopaminergic function and motor behavior during aging. Genes Brain Behav. 2011; 10:186–198. [PubMed: 20860702]

Caccamo A, Majumder S, Richardson A, Strong R, Oddo S. Molecular interplay between mammalian target of rapamycin (mTOR), amyloid-beta, and Tau: effects on cognitive impairments. J Biol Chem. 2010; 285:13107–13120. [PubMed: 20178983]

Chong ZZ, Shang YC, Wang S, Maiese K. Shedding new light on neurodegenerative diseases through the mammalian target of rapamycin. Prog Neurobiol. 2012; 99:128–148. [PubMed: 22980037]

Forgacs B, Merhav HJ, Lappin J, Mieles L. Successful conversion to rapamycin for calcineurin inhibitor-related neurotoxicity following liver transplantation. Transplant Proc. 2005; 37:1912–1914. [PubMed: 15919502]

Fortun J, Dunn WA Jr, Joy S, Li J, Notterpek L. Emerging role for autophagy in the removal of aggresomes in Schwann cells. J Neurosci. 2003; 23:10672–10680. [PubMed: 14627652]

Fortun J, Go JC, Li J, Amici SA, Dunn WA Jr, Notterpek L. Alterations in degradative pathways and protein aggregation in a neuropathy model based on PMP22 overexpression. Neurobiol Dis. 2006; 22:153–164. [PubMed: 16326107]

Fortun J, Verrier JD, Go JC, Madorsky I, Dunn WA, Notterpek L. The formation of peripheral myelin protein 22 aggregates is hindered by the enhancement of autophagy and expression of cytoplasmic chaperones. Neurobiol Dis. 2007; 25:252–265. [PubMed: 17174099]

Hanemann CO, D'Urso D, Gabreels-Festen AA, Muller HW. Mutation-dependent alteration in cellular distribution of peripheral myelin protein 22 in nerve biopsies from Charcot-Marie-Tooth type 1A. Brain. 2000; 123 (Pt 5):1001–1006. [PubMed: 10775544]

Harrison DE, Strong R, Sharp ZD, Nelson JF, Astle CM, Flurkey K, Nadon NL, Wilkinson JE, Frenkel K, Carter CS, Pahor M, Javors MA, Fernandez E, Miller RA. Rapamycin fed late in life extends lifespan in genetically heterogeneous mice. Nature. 2009; 460:392–395. [PubMed: 19587680]

Ichimura Y, Komatsu M. Selective degradation of p62 by autophagy. Seminars in immunopathology. 2010; 32:431–436. [PubMed: 20814791]

Ingram DK, Zhu M, Mamczarz J, Zou S, Lane MA, Roth GS, deCabo R. Calorie restriction mimetics: an emerging research field. Aging Cell. 2006; 5:97–108. [PubMed: 16626389]

Jessen KR, Mirsky R. Schwann cells and their precursors emerge as major regulators of nerve development. Trends Neurosci. 1999; 22:402–410. [PubMed: 10441301]

Kim SG, Buel GR, Blenis J. Nutrient regulation of the mTOR Complex 1 signaling pathway. Mol Cells. 2013

Klionsky DJ, et al. Guidelines for the use and interpretation of assays for monitoring autophagy. Autophagy. 2012; 8:445–544. [PubMed: 22966490]

Koyama S, Hata S, Witt CC, Ono Y, Lerche S, Ojima K, Chiba T, Doi N, Kitamura F, Tanaka K, Abe K, Witt SH, Rybin V, Gasch A, Franz T, Labeit S, Sorimachi H. Muscle RING-finger protein-1 (MuRF1) as a connector of muscle energy metabolism and protein synthesis. J Mol Biol. 2008; 376:1224–1236. [PubMed: 18222470]

Kubota H, Matsumoto S, Yokota S, Yanagi H, Yura T. Transcriptional activation of mouse cytosolic chaperonin CCT subunit genes by heat shock factors HSF1 and HSF2. FEBS Lett. 1999; 461:125–129. [PubMed: 10561509]

Lamming DW, Ye L, Sabatini DM, Baur JA. Rapalogs and mTOR inhibitors as anti-aging therapeutics. J Clin Invest. 2013; 123:980–989. [PubMed: 23454761]

Lee S, Notterpek L. Dietary restriction supports peripheral nerve health by enhancing endogenous protein quality control mechanisms. Exp Gerontol. 2013; 48:1085–1090. [PubMed: 23267845]

Madorsky I, Opalach K, Waber A, Verrier JD, Solmo C, Foster T, Dunn WA Jr, Notterpek L. Intermittent fasting alleviates the neuropathic phenotype in a mouse model of Charcot-Marie-Tooth disease. Neurobiol Dis. 2009; 34:146–154. [PubMed: 19320048]

Malagelada C, Jin ZH, Jackson-Lewis V, Przedborski S, Greene LA. Rapamycin protects against neuron death in in vitro and in vivo models of Parkinson's disease. J Neurosci. 2010; 30:1166–1175. [PubMed: 20089925]

Martini R, Schachner M. Molecular bases of myelin formation as revealed by investigations on mice deficient in glial cell surface molecules. Glia. 1997; 19:298–310. [PubMed: 9097074]

Mattson MP. Dietary factors, hormesis and health. Ageing Res Rev. 2008; 7:43–48. [PubMed: 17913594]

Meekins GD, Emery MJ, Weiss MD. Nerve conduction abnormalities in the trembler-j mouse: a model for Charcot-Marie-Tooth disease type 1A? J Peripher Nerv Syst. 2004; 9:177–182. [PubMed: 15363066]

Meikle L, Pollizzi K, Egnor A, Kramvis I, Lane H, Sahin M, Kwiatkowski DJ. Response of a neuronal model of tuberous sclerosis to mammalian target of rapamycin (mTOR) inhibitors: effects on

mTORC1 and Akt signaling lead to improved survival and function. J Neurosci. 2008; 28:5422–5432. [PubMed: 18495876]

Mizushima N, Yoshimori T. How to interpret LC3 immunoblotting. Autophagy. 2007; 3:542–545. [PubMed: 17611390]

Narayanan SP, Flores AI, Wang F, Macklin WB. Akt signals through the mammalian target of rapamycin pathway to regulate CNS myelination. J Neurosci. 2009; 29:6860–6870. [PubMed: 19474313]

Nicks JR, Lee S, Kostamo KA, Harris AB, Sookdeo AM, Notterpek L. Long-term Analyses of Innervation and Neuromuscular Integrity in the Trembler-J Mouse Model of Charcot-Marie-Tooth Disease. J Neuropathol Exp Neurol. 2013; 72:942–954. [PubMed: 24042197]

Niemann S, Sereda MW, Rossner M, Stewart H, Suter U, Meinck HM, Griffiths IR, Nave KA. The "CMT rat": peripheral neuropathy and dysmyelination caused by transgenic overexpression of PMP22. Ann N Y Acad Sci. 1999; 883:254–261. [PubMed: 10586250]

Nishimura T, Yoshikawa H, Fujimura H, Sakoda S, Yanagihara T. Accumulation of peripheral myelin protein 22 in onion bulbs and Schwann cells of biopsied nerves from patients with Charcot-Marie-Tooth disease type 1A. Acta Neuropathol. 1996; 92:454–460. [PubMed: 8922056]

Notterpek L, Shooter EM, Snipes GJ. Upregulation of the endosomal-lysosomal pathway in the trembler-J neuropathy. J Neurosci. 1997; 17:4190–4200. [PubMed: 9151736]

Pareek S, Notterpek L, Snipes GJ, Naef R, Sossin W, Laliberte J, Iacampo S, Suter U, Shooter EM, Murphy RA. Neurons promote the translocation of peripheral myelin protein 22 into myelin. J Neurosci. 1997; 17:7754–7762. [PubMed: 9315897]

Parzych KR, Klionsky DJ. An Overview of Autophagy: Morphology, Mechanism, and Regulation. Antioxidants & redox signaling. 2013

Quy PN, Kuma A, Pierre P, Mizushima N. Proteasome-dependent activation of mammalian target of rapamycin complex 1 (mTORC1) is essential for autophagy suppression and muscle remodeling following denervation. J Biol Chem. 2013; 288:1125–1134. [PubMed: 23209294]

Rangaraju S, Notterpek L. Autophagy aids membrane expansion by neuropathic Schwann cells. Autophagy. 2011; 7:238–239. [PubMed: 21135575]

Rangaraju S, Verrier JD, Madorsky I, Nicks J, Dunn WA Jr, Notterpek L. Rapamycin activates autophagy and improves myelination in explant cultures from neuropathic mice. J Neurosci. 2010; 30:11388–11397. [PubMed: 20739560]

Ravikumar B, Vacher C, Berger Z, Davies JE, Luo S, Oroz LG, Scaravilli F, Easton DF, Duden R, O'Kane CJ, Rubinsztein DC. Inhibition of mTOR induces autophagy and reduces toxicity of polyglutamine expansions in fly and mouse models of Huntington disease. Nat Genet. 2004; 36:585–595. [PubMed: 15146184]

Rubinsztein DC, Codogno P, Levine B. Autophagy modulation as a potential therapeutic target for diverse diseases. Nat Rev Drug Discov. 2012; 11:709–730. [PubMed: 22935804]

Sarkar S, Rubinsztein DC. Small molecule enhancers of autophagy for neurodegenerative diseases. Mol Biosyst. 2008; 4:895–901. [PubMed: 18704227]

Sherman DL, Krols M, Wu LM, Grove M, Nave KA, Gangloff YG, Brophy PJ. Arrest of myelination and reduced axon growth when Schwann cells lack mTOR. J Neurosci. 2012; 32:1817–1825. [PubMed: 22302821]

Shoji-Kawata S, Sumpter R, Leveno M, Campbell GR, Zou Z, Kinch L, Wilkins AD, Sun Q, Pallauf K, MacDuff D, Huerta C, Virgin HW, Helms JB, Eerland R, Tooze SA, Xavier R, Lenschow DJ, Yamamoto A, King D, Lichtarge O, Grishin NV, Spector SA, Kaloyanova DV, Levine B. Identification of a candidate therapeutic autophagy-inducing peptide. Nature. 2013; 494:201–206. [PubMed: 23364696]

Skre H. Genetic and clinical aspects of Charcot-Marie-Tooth's disease. Clin Genet. 1974; 6:98–118. [PubMed: 4430158]

Srivastava S, Haigis MC. Role of sirtuins and calorie restriction in neuroprotection: implications in Alzheimer's and Parkinson's diseases. Curr Pharm Des. 2011; 17:3418–3433. [PubMed: 21902666]

Suter U, Moskow JJ, Welcher AA, Snipes GJ, Kosaras B, Sidman RL, Buchberg AM, Shooter EM. A leucine-to-proline mutation in the putative first transmembrane domain of the 22-kDa peripheral

myelin protein in the trembler-J mouse. Proc Natl Acad Sci U S A. 1992; 89:4382–4386. [PubMed: 1374899]

Tyler WA, Gangoli N, Gokina P, Kim HA, Covey M, Levison SW, Wood TL. Activation of the mammalian target of rapamycin (mTOR) is essential for oligodendrocyte differentiation. J Neurosci. 2009; 29:6367–6378. [PubMed: 19439614]

Young P, Suter U. The causes of Charcot-Marie-Tooth disease. Cell Mol Life Sci. 2003; 60:2547–2560. [PubMed: 14685682]

Zhang Y, Bokov A, Gelfond J, Soto V, Ikeno Y, Hubbard G, Diaz V, Sloane L, Maslin K, Treaster S, Rendon S, van Remmen H, Ward W, Javors M, Richardson A, Austad SN, Fischer K. Rapamycin Extends Life and Health in C57BL/6 Mice. J Gerontol A Biol Sci Med Sci. 2013

Highlights

- Rapamycin administration is not beneficial for neuromuscular performance in TrJ mice
- Rapamycin treatment supports myelin in 4 and 12 month old neuropathic mice
- Skeletal muscle abnormalities are not attenuated by rapamycin in affected mice
- Peripheral nerves and skeletal muscle respond distinctively to rapamycin

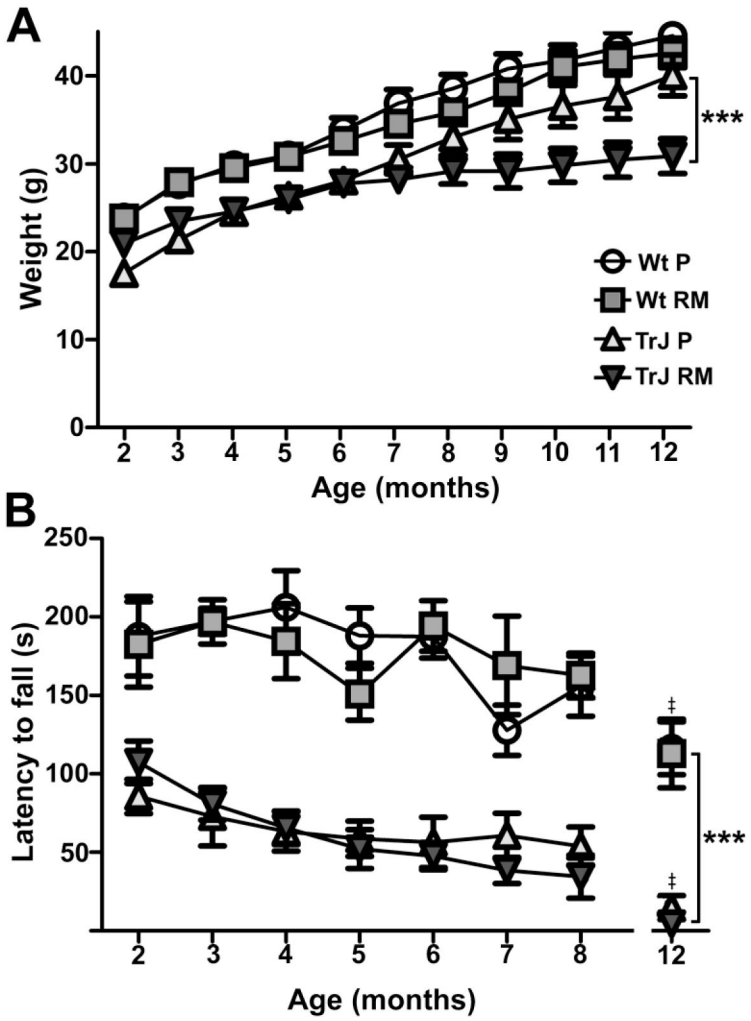

Figure 1. Weight gain and locomotor performance in control and rapamycin-fed Wt and neuropathic mice

(**A**) Wt and neuropathic TrJ mice were administered either rapamycin-enriched (Wt RM; TrJ RM) or placebo (Wt P; TrJ P) diet from 2–12 months of age. Wt mice gained weight at a similar rate regardless of diet. At the end of the study, TrJ mice on the RM-enriched diet had a ~17 % reduction in body weight, compared to placebo (***$p<0.001$). Representative data from 3 independent cohorts is shown. (**B**) Performance of the mice on the rotarod was not affected by the diet. TrJ mice had a significantly shorter latency to fall relative to Wt throughout testing (***$p<0.001$), and both groups showed age-related declines in performance (‡ $p<0.01$). Results were consistent across 3 different cohorts, n=6–8 mice per group.

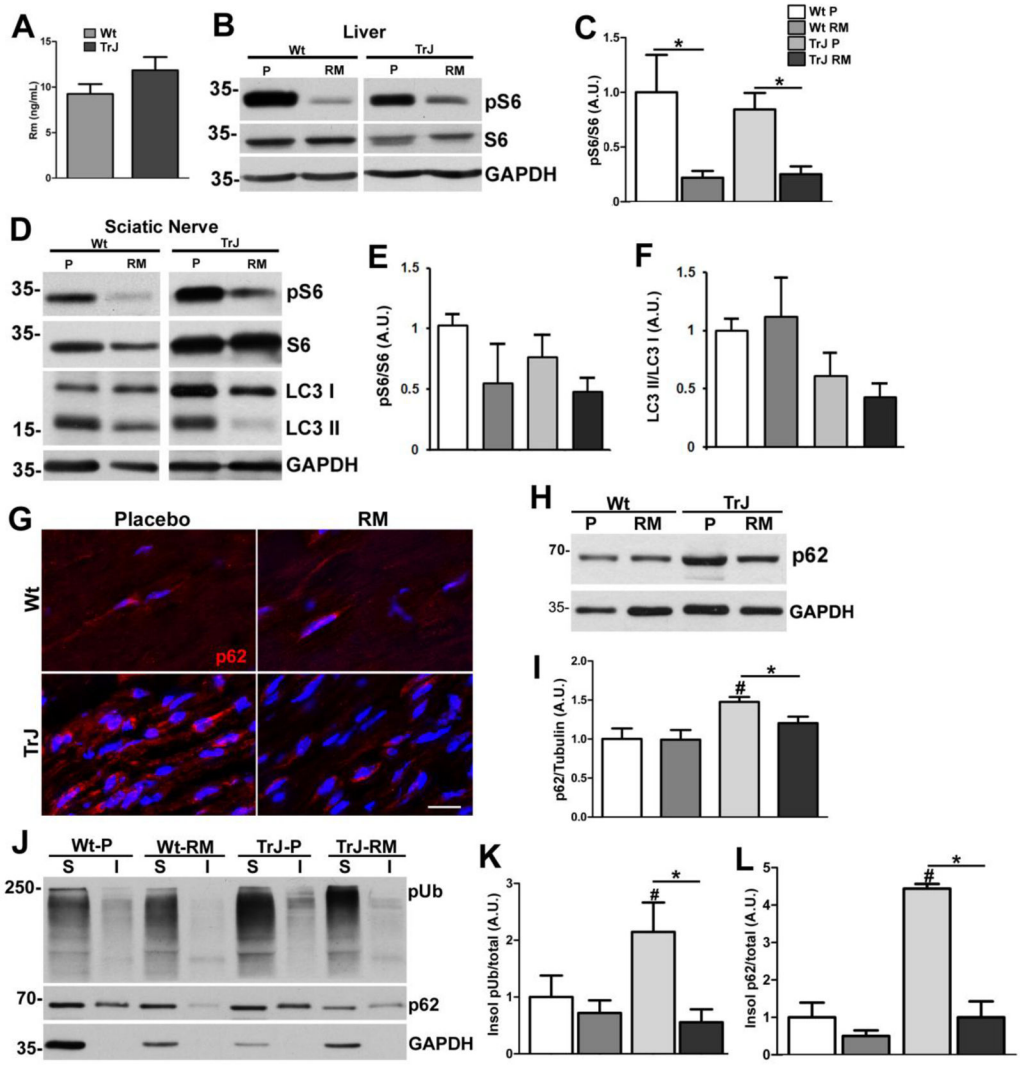

Figure 2. Plasma concentration and bioactivity of rapamycin in target tissues

(**A**) HPLC analysis detected 10–12 ng of RM per ml in the plasma of rapamycin-fed Wt and TrJ mice. Rapamycin levels in placebo-fed mice were below the lower limit of detection (n=8–10 mice/group). (**B**) Whole liver tissue lysates (30 μg/lane) from Wt and TrJ mice on placebo (P) or rapamycin-enriched (RM) chow were probed for pS6 and total S6. (**C**) Statistical analyses of pS6 to total S6 ratios after correction for GAPDH from 4 independent experiments. (**D**) Whole sciatic nerve lysates (30 μg/lane) were probed for pS6, total S6, and LC3. Semi-quantitative analyses of pS6 to total S6 (**E**), and LC3 II to LC3 I ratios (**F**), from nerve blots after correction for GAPDH from 4 independent experiments. (**G**) Cryosections of sciatic nerves from the indicated animals were immunolabeled with an anti-p62 antibody and Hoechst dye. (**H**) Western blot analysis of nerve lysates with the same anti-p62 antibody is shown. (**I**) Statistical analyses of p62 levels after correction for tubulin from 4 independent experiments. (**J**) Sciatic nerve lysates from placebo and rapamycin-fed Wt and TrJ mice were separated into detergent-soluble (S) and -insoluble (I) fractions, and probed for pUb, and p62. Representative blots, 3 independent experiments. GAPDH is shown as a

protein loading control (**B, D, H, J**). Molecular mass, in kDa (**B, D, H, J)**. (**K. L**) Statistical analyses of insoluble, relative to total, pUb and p62 from 3 independent experiments are shown. Genotype effect is indicated with # $p<0.05$. *$p<0.05$; A.U.; arbitrary units;

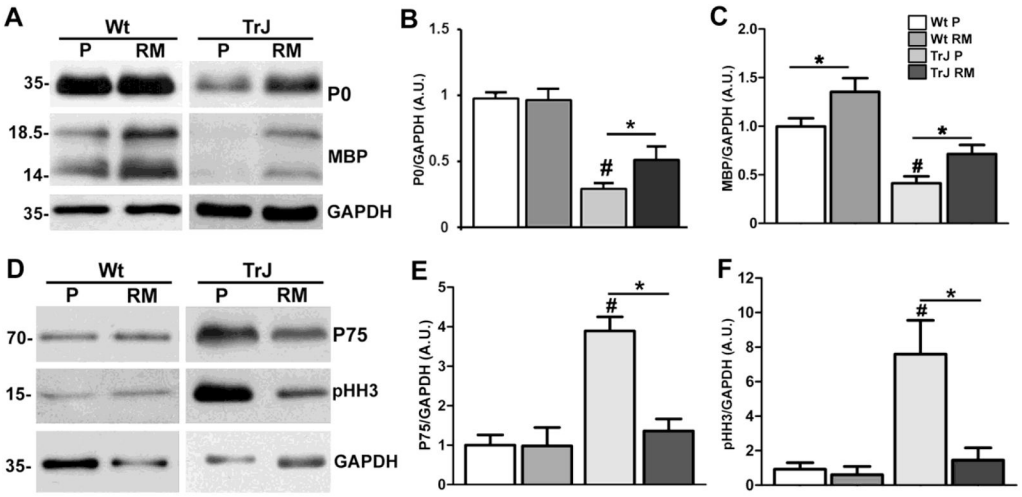

Figure 3. Rapamycin supplementation supports the myelinated Schwann cell phenotype

(A) Whole nerve lysates (20 μg/lane) from placebo (P) and rapamycin-fed (RM) Wt and TrJ mice were assessed for the expression of myelin proteins P0 and MBP. Representative blots, 5 independent experiments. (**B, C**) Statistical analyses of P0 and MBP from 5 independent blots. The levels of P0 and MBP are significantly lower in nerves of TrJ mice on the placebo regimen (#$p<0.01$) as compared to Wt. (**D**) The same sciatic nerve lysates (20 μg/lane) were probed for the neurotrophin receptor P75 and the mitotic marker pHH3. Representative blots, 3 separate experiments. (**E, F**) Analyses of P75 and pHH3 levels after correction for GAPDH show an effect of genotype (# $p<0.01$) across placebo fed mice, and attenuation of neuropathic phenotype after rapamycin feeding. Quantification is based on 3 independent blots.

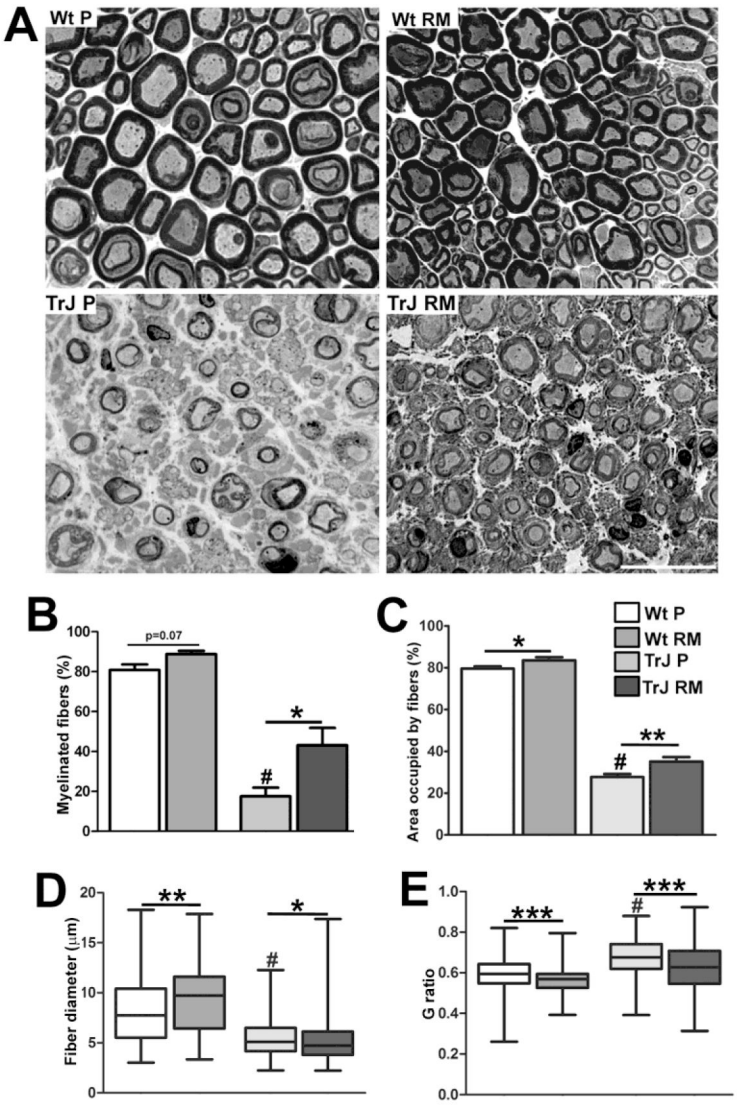

Figure 4. Morphometric analyses of sciatic nerves from placebo and rapamycin-fed mice

(**A**) Cross-sectional views of proximal sciatic nerve segments from Wt and TrJ mice fed either placebo (P) or RM-enriched diet (RM) are shown. Micron bar, 25 μm. (**B–E**) Morphometric analyses of at least 200 fibers per nerve segments from 4 individual Wt and TrJ mice from each group. For all 4 measurements a genotype effect is observed (#p<0.001). (**B**) There is a significant (*p<0.05) increase in the percentage of myelinated fibers in nerves from TrJ mice on the rapamycin-enriched diet. (**C**) The total nerve tissue area occupied by fibers in a fixed field of view show significant improvements in Wt (*p<0.05), as well as TrJ (**p<0.01) mice on the rapamycin diet. (**D**) Measurements of fiber diameters show increases in nerves of Wt (**p<0.01) and decreases in TrJ (*p<0.05) on the intervention. (**E**) Quantification of the G ratios indicate highly significant (***p<0.001) changes in both Wt and TrJ mice on the rapamycin-enriched diet.

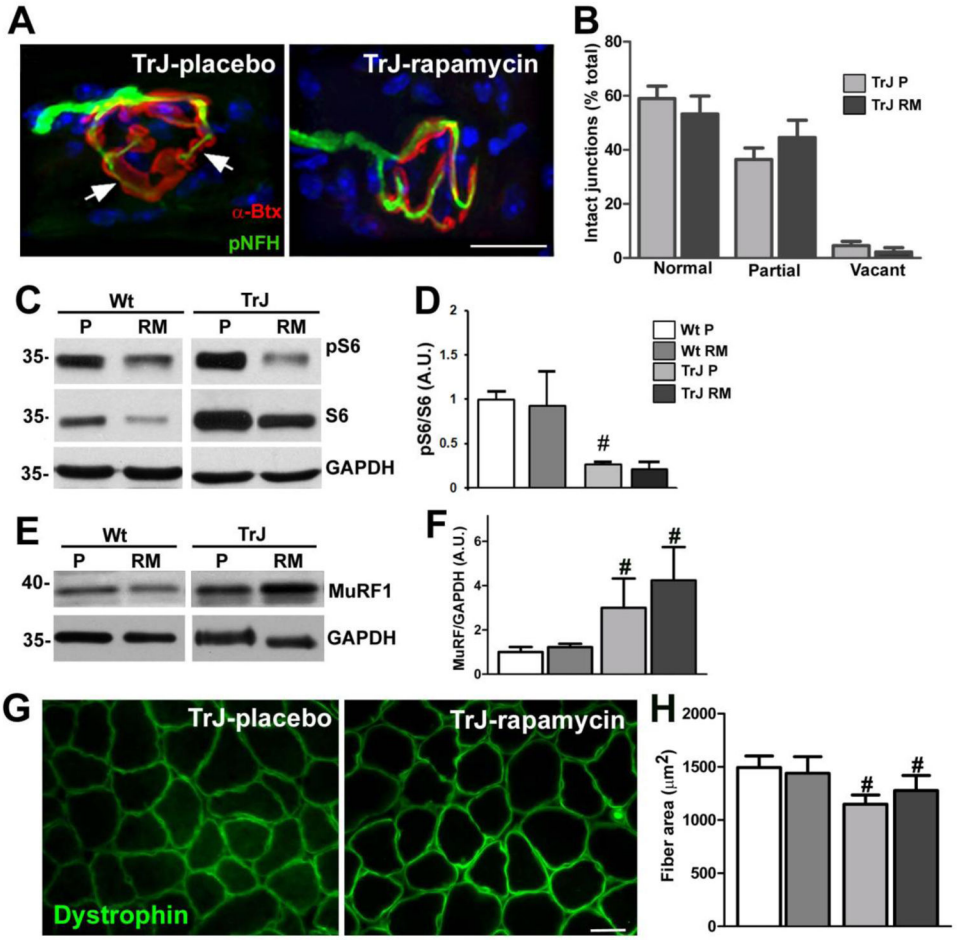

Figure 5. Rapamycin was ineffective in attenuating skeletal muscle abnormalities in neuropathic mice

(**A**) Neuromuscular integrity was analyzed using an NFH antibody to label the pre-synaptic nerve terminal and α-Btx to identify post-synaptic acetylcholine receptors. Arrows denote thinning nerve terminals. Nuclei are stained with Hoechst dye. (**B**) The integrity of the neuromuscular junctions in soleus muscles from TrJ mice were recorded as normal (N), partially innervated (P) or vacant (V). At least 30 neuromuscular junctions were analyzed for each group. (**C**) Whole soleus muscle lysates (30 μg/lane) from Wt and TrJ mice fed either placebo (P) or rapamycin-enriched diet (RM) were assessed for inhibition of mTOR using antibodies against pS6 and S6. Representative blot, 4 independent experiments. (**D**) Statistical analyses of pS6 to total S6 ratios after correction for GAPDH from 4 independent experiments. (**E**) Anti-MuRF1 antibody was used to assess muscle atrophy. Representative blots, 4 individual experiments. Molecular mass, in kDa (**C,E**). (**F**) Analysis of MuRF levels after correction for GAPDH shows an effect of genotype (# $p<0.01$). Quantification is based on 4 independent blots. A.U.; arbitrary units. (**G**) Muscle fiber morphology was evaluated using an anti-dystrophin antibody. (**H**) The rapamycin-enriched diet had no effect on muscle fiber cross-sectional area. At least 30 fibers from 3 different animals per group were analyzed. Genotype effect is indicated with # $p<0.05$. (**A,G**) Micron bar, 10μm.

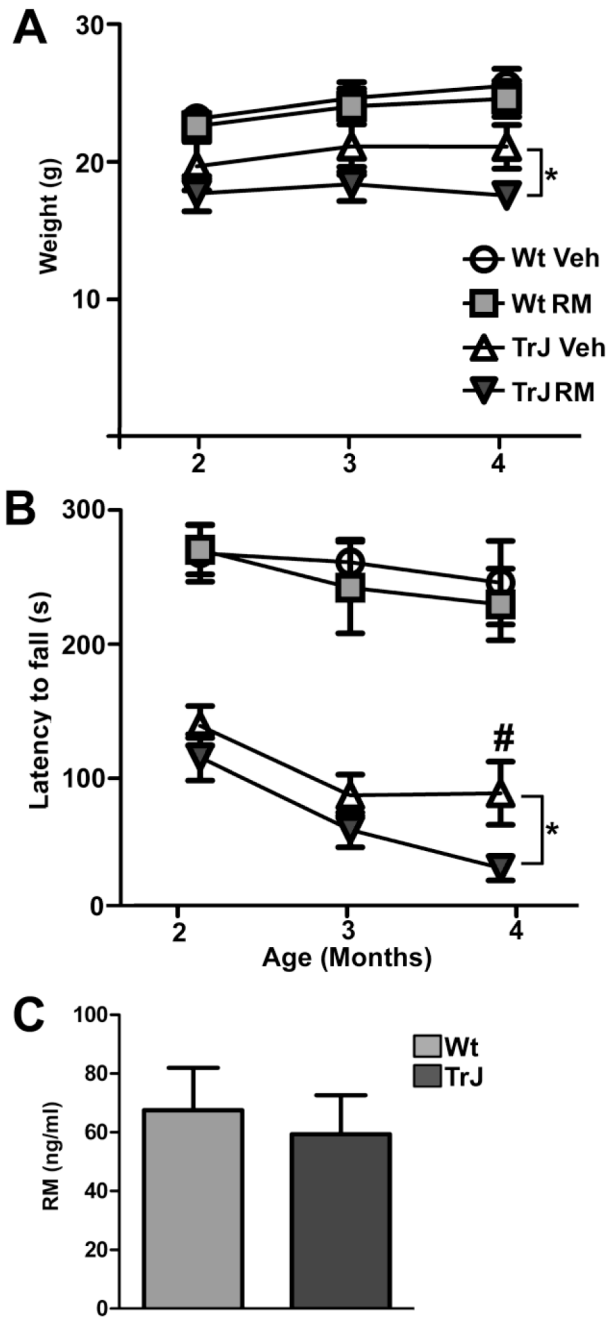

Figure 6. Body weight and locomotor performance in control and rapamycin-injected Wt and TrJ mice

(**A)** Wt and TrJ mice received rapamycin (6 mg/kg) or vehicle (V) injections beginning at 2 month of age and body weights were measured weekly. At 4 months of age, rapamycin-injected animals show a significant (*$p<0.05$) reduction in body weight. (n=5–8 mice per group). (**B**) Performance of Wt mice on the rotarod was not affected by rapamycin; however, compound treated TrJ mice show a significant decline in latency to fall as compared to vehicle injected littermates (*$p<0.05$). Genotype effect is indicated with # $p<0.01$. Results were consistent across 3 different trials. (**C**) HPLC analysis of serum

detected over 60 ng/ml of rapamycin in injected mice (n=5–8 plasma samples from individual mice per group.)

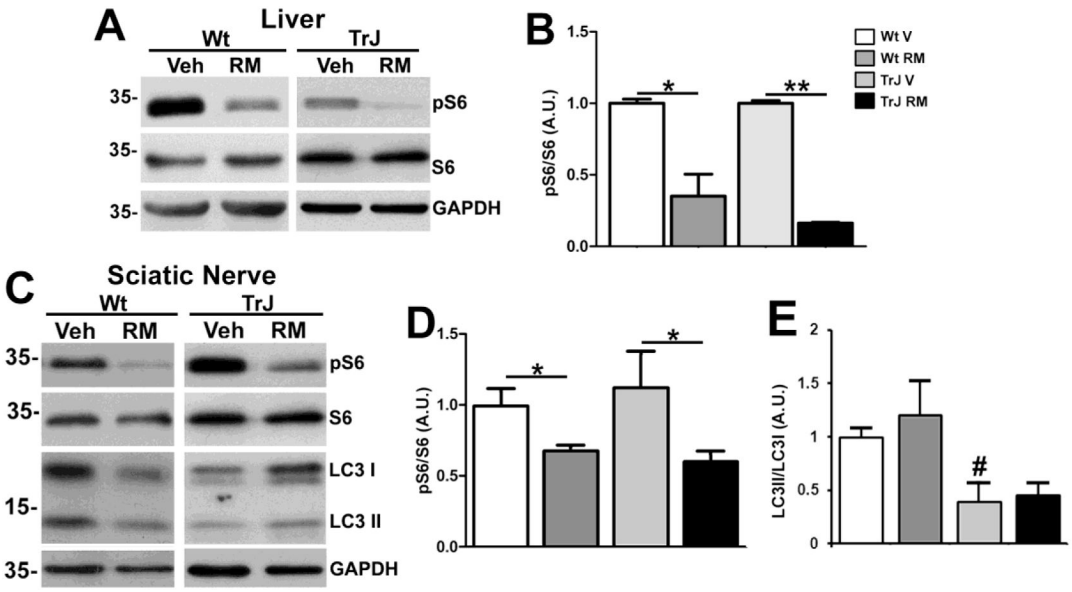

Figure 7. Bioactivity of rapamycin in the liver and sciatic nerve of injected mice

(**A**) Whole liver tissue lysates (30 μg/lane) from rapamycin (6 mg/kg, RM) or vehicle-injected (V) mice were probed for pS6 and total S6. GAPDH is shown as a protein loading control. Representative blots, 4 experiments. (**B**) Analyses of pS6 to total S6 ratios in liver tissue after correction for GAPDH from 4 independent experiments. (**C**) Whole sciatic nerve tissue lysates (30 μg/lane) from rapamycin (6 mg/kg) or vehicle-injected mice were probed for pS6 and total S6, and for the autophagy protein LC3. Representative blots, 4 experiments. (**A,C**) Molecular mass, in kDa. (**D, E**) Analysis of pS6 to total S6, and LC3 II to LC3 I, ratios after correction for GAPDH from 4 independent experiments. Genotype effect is indicated with # $p<0.05$. *$p<0.05$; **$p<0.01$; A.U.; arbitrary units.

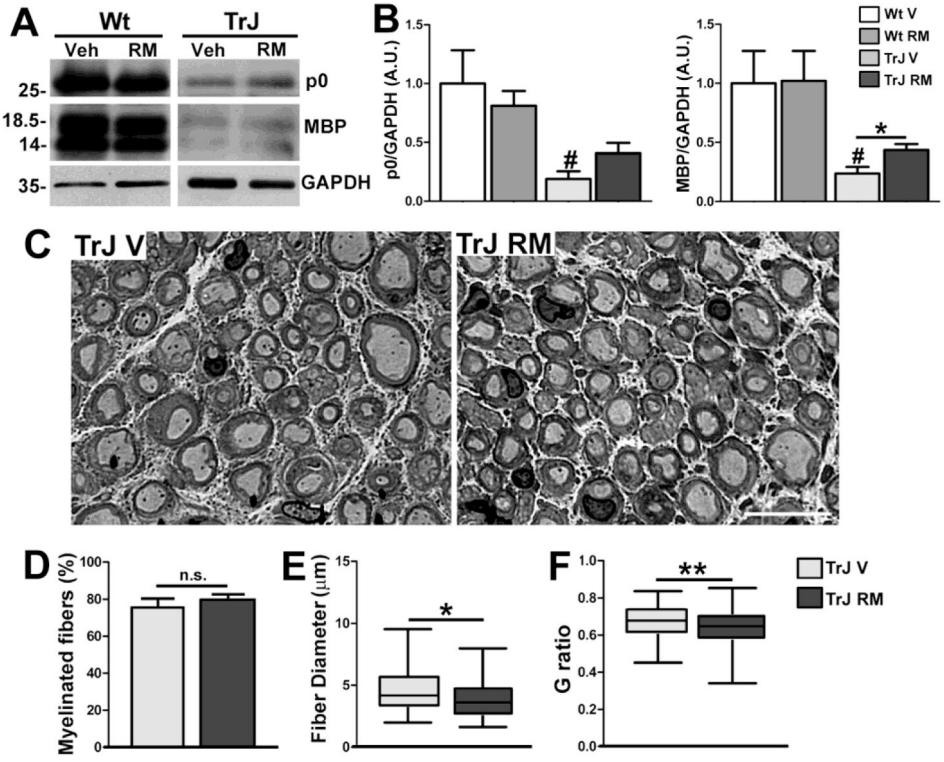

Figure 8. Biochemical and morphological assessment of myelinated nerves in rapamycin-injected mice

(**A**) Whole sciatic nerve lysates (20 μg/ml) from Wt and TrJ mice injected with vehicle (V) or rapamycin (RM) were probed for the myelin proteins P0 and MBP. GAPDH is shown as a protein loading control. Molecular mass, in kDa. (**B**) Analyses of P0 and MBP from 4 independent blots. The levels of P0 and MBP are significantly lower in nerves of TrJ mice on the placebo regimen (#$p<0.01$) as compared to Wt. (**C**) Cross-sections of sciatic nerves from TrJ mice administered vehicle (V) or 6 mg/kg of rapamycin (RM). Micron bar, 25 μm. (**D**) The percentage of myelinated fibers did not change significantly in response to rapamycin injection. n.s. non-significant. (**E**) Measurements of fiber diameters show a significant decrease in nerves of rapamycin-injected TrJ mice. (**F**) Quantification of the mean G ratios, calculated as axon diameter divided by fiber diameter, show significant decrease in rapamycin-injected TrJ mice. For all morphometric analyses at least 50 fibers from the nerve segments of 4 individual TrJ mice were analyzed. *$p<0.05$; **$p<0.01$.

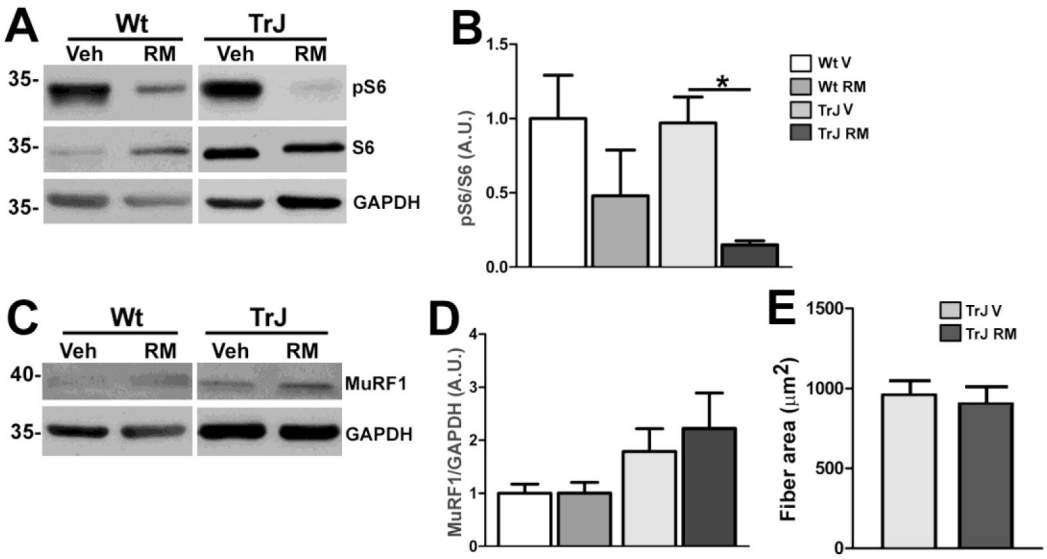

Figure 9. The effects of high circulating rapamycin on soleus muscle

(**A**) Whole soleus muscle lysates (30 μg/lane) from Wt and TrJ mice injected with either vehicle (V) or rapamycin (RM) were probed with anti-pS6 and S6 antibodies. Representative blot, 4 independent experiments. (**B**) Analyses of pS6 to total S6 ratios after correction for GAPDH from 4 independent experiments (*$p<0.05$). (**C**) Western blotting with anti-MuRF1 antibody was used to assess muscle atrophy. Representative blots, 4 individual experiments. (**A, C**) Molecular mass, in kDa. (**D**) Analysis of MuRF levels after correction for GAPDH. Quantification is based on 4 independent blots. (**E**) Soleus muscle fiber cross-sectional area was evaluated after immunostaining with an anti-dystrophin antibody. At least 30 fibers from 3 different animals per group were analyzed.